International Journal of Innovative Technology and Exploring Engineering (IJITEE)
ISSN: 2278-3075 (Online), Volume-9 Issue-2, December 2019

Optimizing Sensor Relationship for Fusion of Multispectral and Panchromatic Imagery

Vaibhav R. Pandit, R. J. Bhiwani

Abstract*: The remote sensing satellite products: multispectral and panchromatic imagery are characterized by different levels of spatio-spectral resolutions. The fusion of these two images (provided, they are acquired for same geographic scenario) is also known as 'Pansharpening'. This produces a composite image featuring simultaneous high levels of spatio-spectral resolutions to meet the demand of the most of remote sensing applications. Thus, different approaches for such fusion and further its quality assessment are continuously researched. The modulation transfer function is unique to the imaging sensors. In this paper, the sensor relationship of the input imagery is optimized to produce the efficient pansharpened/fused image. The performance measurement is carried out on two real datasets made available by WorldView-2 and WorldView-3 satellite sensors using two assessment techniques. The results of optimization approach are further compared to nine different most recent fusion algorithms.

Keywords* : Image fusion, multispectral image, optimization, panchromatic image.

I. INTRODUCTION

The fusion of multispectral (MS) image (i.e. spectrally-rich and spatially-deficient) with panchromatic (PAN) image (i.e. spatially-rich and spectrally-deficient), those are acquired on the same location by optical remote sensing satellites produces a compound image rich with both spatial and spectral resolutions [1]. Mostly, the spatial richness of PAN image is four-times greater than that of MS image. On the another hand, MS image usually features maximum eight spectral components over visual and near-infrared wavelengths separately as compared to single band of PAN image. The physical constraints of satellite sensors cannot provide unique product rich in both spatial and spectral resolutions. But, the demand for higher spatial as well as higher spectral resolutions is continuously growing for several remote sensing tasks. The promising way to fulfill this demand is seen in terms of 'image fusion' [2] which is also referred as 'Pansharpening'. Detailed literature of image fusion algorithms is surveyed in [3]–[5]. The algorithms are mostly categorized under Component Substitution (CS) [6], Multi-Resolution Analysis (MRA) [7] and hybrid approaches.

Revised Manuscript Received on December 30, 2019.
***** Correspondence Author
Vaibhav R. Pandit*, Research Scholar, Engineering & Technology, Sant Gadge Baba Amravati University, Amravati, Maharashtra State, India.
Dr. R. J. Bhiwani, Professor, Dept. of Electronics & Telecomm. Engg., Babasaheb Naik College of Engineering, Pusad, Maharashtra State, India.

These various ideas of image fusion try to fulfill the demands of remote sensing application tasks which help groundwater prospects mapping, forecast of agricultural output, forest cover mapping, snow & glacier studies, wasteland mapping, object recognition [8], change detection [9], scene interpretation [10] and visual image analysis, etc.

The optimization techniques are popular for providing improvised results using iterations. Though these techniques have proved themselves very potential mathematical procedures and now popular in many research areas, these have been very rarely utilized for producing image fusion results. With respect to MS images, Modulation Transfer Functions (MTFs) are basically figured around gaussian filter having logical formulation completely expressed by the sensor gain at the Nyquist frequency. The works of [11], [12] underline inadequacy of MTFs of the MS sensor those were conventionally used for finding functional relationship of MS to PAN images and further highlight the need of sophisticated optimization of sensor relationship for image fusion. Also, for image fusion researched with diverse approaches, no two ideas can be best compared unless and until the universally accepted standard image data sets, uniform platform for standardized implementations of algorithms and unique evaluation criteria are available. This all motivates the authors to implement image fusion algorithm using optimization technique and compare the obtained results with those of other best known algorithms using standardized platform and real image datasets with proper assessment techniques.

The subsequent portion of this paper is presented as: Section II briefs optimization based image fusion procedure. Application of fusion algorithms to image datasets is made in section III. A discussion on results is addressed in Section IV. Lastly, conclusion is noted in Section V.

II. METHODOLOGY

The conventional CS approach is mathematically represented as follows:

$$F = M_{up} + g(P - I_L) \quad (1)$$

Where, P is the PAN image, M_{up} is the MS image interpolated to the size of P, F is result of image fusion and g is the gain factor for spectral bands $(i = 1,...,n,...,N)$ in MS image. I_L is the synthetic intensity component representing spatial structure of MS image derived from the its spectral components as under:

$$I_L = \sum_{i=1}^{N} w_i (M_{up})_i \quad (2)$$

N in (2) denote total number of frequency bands of MS image overlapped by PAN image. w is a weighting factor for i^{th} band calculated by multiple regression of PAN and MS image. The mathematical representation of CS approach is based on a theme to transform MS image into other domain, with the assumption that the spatial-detail separates itself from the spectral information of image. A component having the spatial contents is thus subsequently swapped by the histogram matched PAN image. Further, through reverse transformation, data is brought back to original space.

Another popular conventional alternative is MRA approach and mathematically described as under:

$$F = M_{up} + g(P - P_L) \quad (3)$$

Where, the meanings of M_{up}, P, F lies the same. P_L is the low-pass form of PAN and computed as:

$$P_L = \sum_{k=1}^{N} w_k (M_{up})_k \quad (4)$$

w in (4) represents optimal weights for spectral bands of MS image denoted as $i = 1,...,N$. The MRA approach to image fusion relies on iterative decomposition scheme that constructs an order of 2D-signals holding progressive reduced contents, which is obtained by the exploitation of particular analysis operators in repeatable manner. Here, the result of image fusion exploits computation of subtracting the low-pass filtered PAN image from itself as shown in (3).

The optimization based image fusion procedure is implemented using MRA approach. The optimization of sensor relationship among input images is defined according to [12] and mathematically expressed in terms of a degradation filter function H as shown below.

$$H = F^{-1}\{\mathrm{o}\frac{A}{B + \lambda + \mu(C + D)}\mathrm{o}\} \quad (5)$$

Where,

$$A = F\{P\}^* \mathrm{o} F\{P_L\} \quad (6)$$

$$B = F\{P\}^* \mathrm{o} F\{P\} \quad (7)$$

$$C = F\{D_h\}^* \mathrm{o} F\{D_h\} \quad (8)$$

$$D = F\{D_v\}^* \mathrm{o} F\{D_v\} \quad (9)$$

Equations (6)-(9) use $F\{\bullet\}$ to indicate the 2D Discrete Fourier Transformation (i.e 2D DFT), $F\{\bullet\}^*$ for the complex conjugate of 2D DFT and o for element wise multiplication of matrices. Here, D_h and D_v involved in (8) and (9) are the block circulant with circulant blocks (BCCB) matrices representing the first-order finite difference operator following horizontal and vertical directions, separately. Substitutions from (6)-(9) to equation (5) results the optimized degradation function H. λ along with μ contribute as the regularizer weights and $F^{-1}\{\bullet\}$ refers for inverse 2D Discrete Fourier Transform. Here, $\mathrm{o}-\mathrm{o}$ denotes the element wise division of matrices.

Downsampling and further interpolation are usually done for computation of gain g. Now, g can be set as (M_{up}/P_L) to make fusion approach as High-Pass Modulation (HPM) injection model. The image fusion algorithm is denoted as 'Opt-Fus' in subsequent sections and is summarized in following steps:

Algorithm: Opt-Fus

Input: M_{up}, P **Output:** F

Step-1: Equalize P to match M_{up} scale.

Step-2: Define filter H as per (5).

Step-3: P_L = Filter P using H.

Step-4: Downsample P_L.

Step-5: Interpolate P_L by 23-coeff. polynomial.

Step-6: Compute g for HPM injection model

Step-7: Obtain F as per (3).

III. EXPERIMENTAL RESULTS

The performance evaluation of Opt-Fus algorithm along with its comparison to performances of CS based image fusion algorithms viz. Intensity-Hue-Saturation (IHS) Transform [13], Nonlinear Intensity-Hue-Saturation (NIHS) [14], Gram-Schmidt Adaptive (GSA) [15], Partial Replacement Adaptive Component Substitution (PRACS) [4], SEGM [16], [17] and MRA based algorithms listed as High Pass Filtering (HPF) [4], [18], Modulation Transfer Function-Generalized Laplacian Pyramid (MTF-GLP) [4], [19]–[21], Indusion [4], [22] and Morphological Half-Gradient (MF-HG) [23], [24] is reported in this section. Two remotely sensed image datasets acquired by two different satellite sensors are used in experimentation. The performance is measured using MATLAB R2019a on the system configuration of core i5 3rd generation processor with 6 GB RAM.

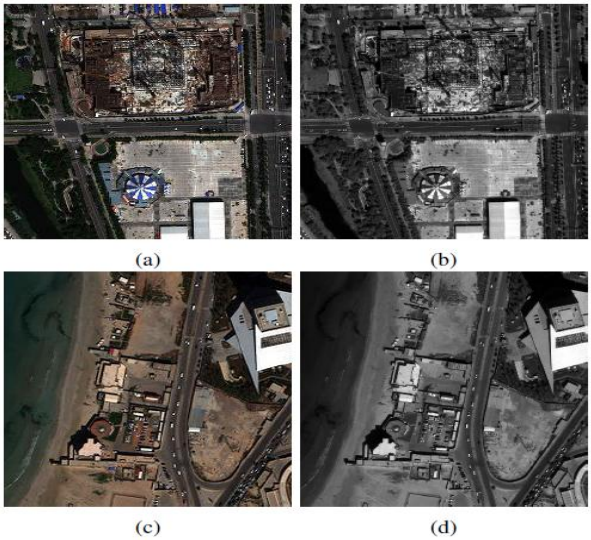

Fig. 1.Dataset-1: Beijing (a) MS and (b) PAN images. Dataset-2: Tripoli (c) MS and (d) PAN images. (Spectrally, only R, G, and B is used for display of MS images.)

A. Datasets

Fig. 1 shows MS and PAN images from the two datasets utilized for experimentation. The other details of datasets are shown in Table I.

Table- I: Dataset Specifications for WorldView-2 and WorldView-3 imagery

Specifications	Dataset-1: Beijing	Dataset-2: Tripoli
Satellite Sensor	WorldView-2	WorldView-3
Spectral Bands	4 MS ; PAN	4 MS ; PAN
Spatial Resolutions	MS: 2 m and PAN: 50 cm	MS: 1.2 m and PAN: 30 cm
Location	Beijing, China	Tripoli, Libya
Data Format	11-bit	11-bit
Provided by	[25]	[26]

Here, MS images of both the datasets hold four spectral bands viz. Blue (B): 450 - 510 nm, Green (G): 510 - 580 nm, Red (R): 630 -690 nm, Near-IR1 (NIR1): 770 - 895 nm); while the single band of PAN image covers 450 - 800 nm. Performance evaluation is carried on a selected region of size 256×256 pixels for MS and 1024×1024 pixels for PAN image of both the datasets.

B. Experimentation and Performance Measurement

For the two datasets, we perform two experiments applying the image fusion algorithms to WorldView-2 and WorldView-3 images. The PAN to MS ratio considering spatial resolutions is 4. Result images after fusion are displayed in Fig. 2 and Fig. 3 for two datasets respectively.

The performances of applied image fusion algorithms are quantified by measurement of quality metrics. The numerical values for Quality w/ No Reference (QNR) [27], Spectral Distortion (D_λ) [27], Spatial Distortion (D_S) [27] and Spectral Angle Mapper (SAM) [27], [28] are obtained using Full-Resolution assessment [29], whereas Root Mean Square Error (RMSE) [28], *Erreur Relative Global Adimensionnelle De Synthese* (ERGAS) [27], [28], Spatial Correlation Coefficient (SCC) [30] and Quality index Q4 [27], [28] are computed using Reduced-Resolution assessment [29]. Table II shows all these quality metric values for experimentation with Dataset-1: Beijing. Table III correspondingly show performance metric values for experimentation with Dataset-2: Tripoli.

IV. ANALYSIS

The previous section reported quantitative results obtained corresponding to the performances of ten image fusion algorithms. Now, the quantitative and qualitative analyses carried on the obtained results are discussed as under:

A. Quantitative Analysis

Using the Full-resolution assessment procedure, we have obtained D_λ, D_S, QNR and SAM. D_λ represents spectral distortion and it is a measure of loss. A comparison of average D_λ values computed on both the datasets can be seen in Fig. 4. Whereas, a comparison of spatial distortion in resultant images can be seen in terms of average D_S values in Fig. 5. Both of these distortions are ideally undesired in resultant images producing values to be 0.

These distortions further contribute to a hybrid quality metric QNR, whose desired value is ideally 1. A comparison of average QNR value calculated on both the datasets with respect to performances of all the fusion algorithms is plotted in Fig. 6. To observe the comparative plot, it is noticed that Opt-Fus is successful to improve this quality metric than those of GSA and MTF-GLP. Its performance is competitive to those of HPF, MF-HG, IHS, SEGM. NIHS, Indusion and PRACS have resulted comparatively superior values.

The desired SAM index is ideally zero. Measurements of average SAM are compared in Fig. 7. The comparison shows Opt-Fus outwitting the performances of SEGM, GSA, IHS, PRACS, NIHS and MF-HG. Here, image fusion using Indusion, MTF-GLP and HPF are found successful in calculating lower value of SAM.

Based on the reduced-resolution assessment technique used in experimentation, a further comparison can be continued for average RMSE values plotted in Fig. 8. The Opt-Fus calculates this error metric superior than those calculated by SEGM, GSA, Indusion and MF-HG. The adaptive fusion algorithm PRACS has resulted in overall the most lower value. Next to it, we find NIHS, HPF and MTF-GLP performing superior than Opt-Fus. Along with RMSE, we calculate ERGAS again an error value, whose comparison is plotted in Fig. 9. As ERGAS is using RMSE value in its calculation, we notice very similar trend of performances of image fusion algorithms.

SCC computes percentage of spatial details injected to final resultant images. A comparison of average SCC values is plotted in Fig. 10. Here, Opt-Fus has better results than those of SEGM, GSA, IHS and NIHS. Indusion and Opt-Fus have performed very very similar in calculating average SCC metric. On further comparison PRACS, MTF-GLP, MF-HG and HPF have achieved superior SCC than that of Opt-Fus.

A quality content among the fused images can also be measured in terms of Q4 index. Average Q4 index is plotted against image fusion algorithms and the plot is shown in Fig. 11. Here, Opt-Fus proved its potential against SEGM, GSA, IHS, Indusion, MF-HG, MTF-GLP. PRACS, NIHS and HPF are found with good values achieved for Q4.

Finally, a comparison of average time taken by image fusion algorithms to generate high resolution resultant image is plotted in Fig. 12. IHS and HPF being simplest in their structures, have resulted with very fast fusion results. Opt-Fus comparatively has taken considerable time to perform image fusion, but is very economical than NIHS.

B. Visual Inspection

The variations in values corresponding to quality- and error-metrics analyzed in previous subsection underline the suitability of metrics to image fusion algorithms still being an open research problem. Also, user is the ultimate judge of results at end use. Hence, a

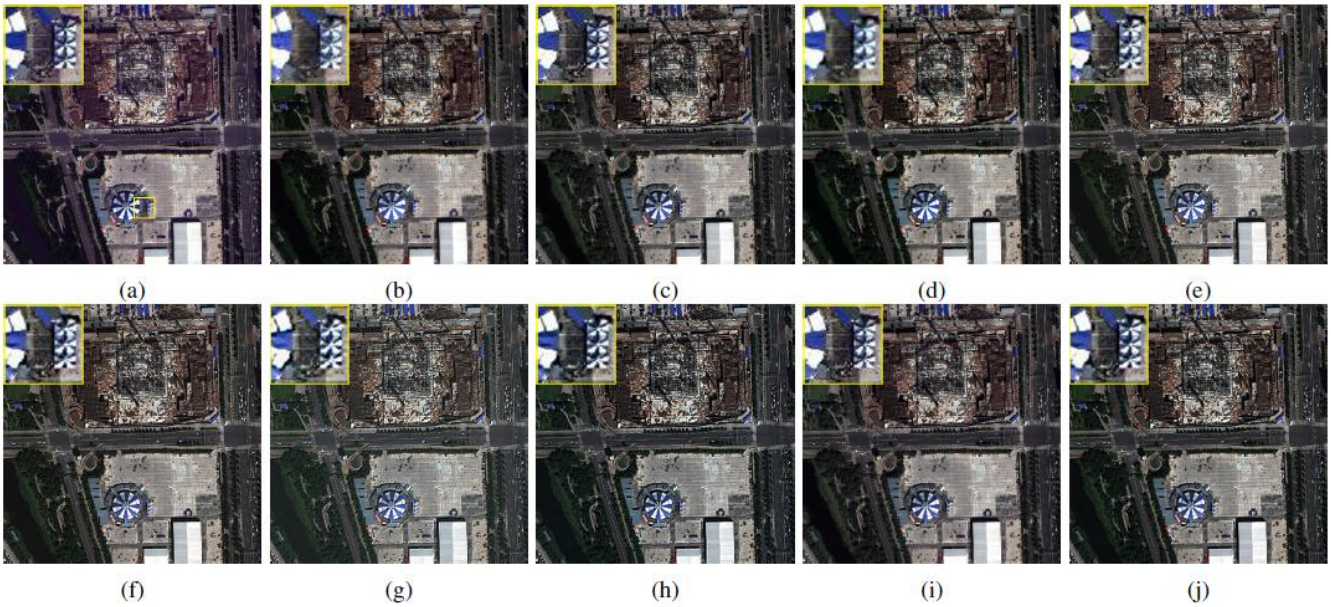

Fig. 2.Experimentation with Dataset-1: Beijing. Resultant fused images of (a) IHS, (b) NIHS, (c) GSA, (d) PRACS, (e) HPF, (f) MTF-GLP, (g) Indusion, (h) MF-HG, (i) SEGM, (j) Opt-Fus. (The spectral band combination of only R, G, and B is used for display purpose. The magnification of a region outlined in (a) is represented at top left in every fused image to help visual distinction.)

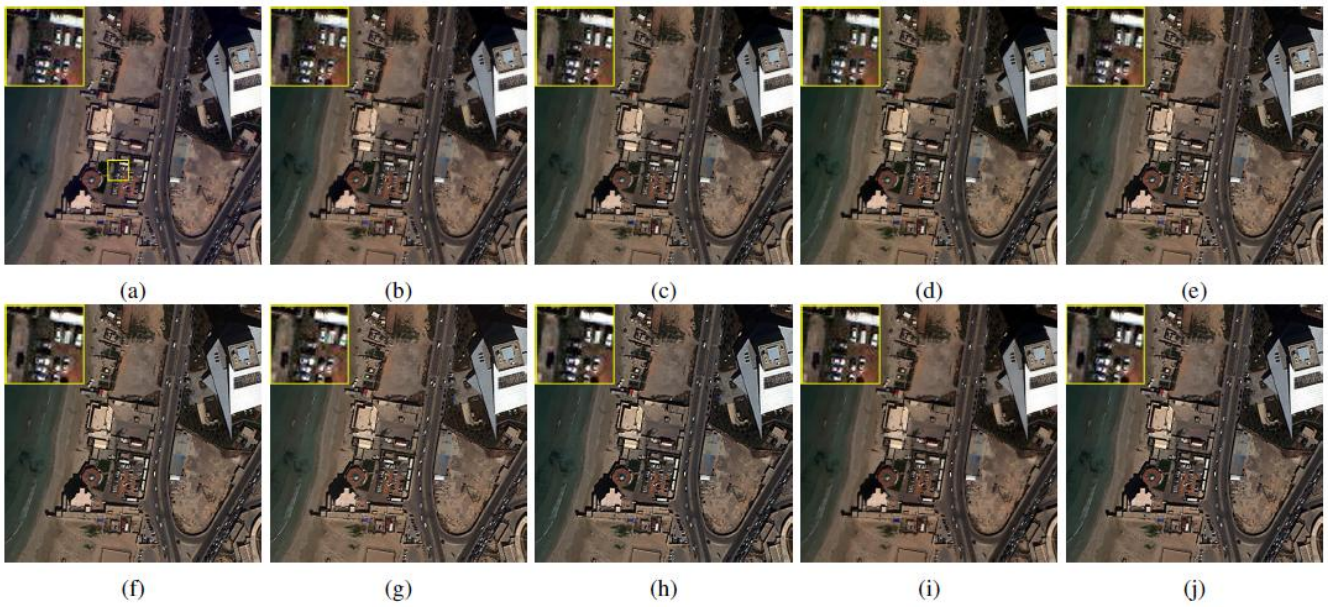

Fig. 3.Experimentation with Dataset-2: Tripoli. Resultant fused images of (a) IHS, (b) NIHS, (c) GSA, (d) PRACS, (e) HPF, (f) MTF-GLP, (g) Indusion, (h) MF-HG, (i) SEGM, (j) Opt-Fus. (The spectral band combination of only R, G, and B is used for display purpose. The magnification of a region outlined in (a) is represented at top left in every fused image to help visual distinction.)

Table- II: Measurement of performance metrics and Execution Time for Dataset-1: Beijing.

Algorithm	Full Resolution Assessment				Reduced Resolution Assessment				Time (s)
	QNR	D_λ	D_S	SAM $(^\circ)$	RMSE	ERGAS	SCC	Q4	
IHS	0.8091	0.0284	0.1673	3.5494	84.3609	5.6217	0.5573	0.6813	0.0464
NIHS	0.8567	0.0095	0.1351	3.3589	57.8671	3.8416	0.7273	0.8427	14.5009
GSA	0.7464	0.0702	0.1972	3.8303	104.9175	6.9221	0.5383	0.6493	0.7854
PRACS	0.8231	0.0202	0.1599	3.3816	48.0126	3.3842	0.8104	0.8772	1.4053

HPF	0.7785	0.0697	0.1632	3.2319	81.4092	5.2593	0.6884	0.7789	0.2525
MTF-GLP	0.7717	0.0807	0.1606	3.1943	87.3196	5.6411	0.7038	0.7684	1.3098
Indusion	0.8422	0.0633	0.1009	2.8383	104.3066	6.7126	0.6746	0.7000	0.5486
MF-HG	0.7883	0.0864	0.1371	3.2786	97.8561	6.3905	0.7067	0.7553	0.6874
SEGM	0.7882	0.0855	0.1381	4.2391	112.7884	7.5429	0.5187	0.6179	0.3964
Opt-Fus	0.7750	0.0777	0.1597	3.2460	91.2091	5.9556	0.6789	0.7665	2.2400

Table- III: Measurement of performance metrics and Execution Time for Dataset-2: Tripoli.

Algorithm	Full Resolution Assessment				Reduced Resolution Assessment				Time (s)
	QNR	D_λ	D_S	SAM $(^o)$	RMSE	ERGAS	SCC	Q4	
IHS	0.8143	0.0709	0.1236	2.1020	79.2267	3.8453	0.5944	0.7193	0.0606
NIHS	0.9043	0.0425	0.0555	2.0597	70.8334	3.3955	0.6339	0.8095	15.6032
GSA	0.8108	0.0728	0.1256	2.4413	91.8524	4.3192	0.5752	0.6980	0.7863
PRACS	0.8787	0.0318	0.0924	2.0617	68.9844	3.1711	0.6749	0.8205	1.3823
HPF	0.8292	0.0789	0.0998	1.9422	69.9803	3.2890	0.7124	0.7988	0.2534
MTF-GLP	0.8242	0.0911	0.0932	1.9379	78.7433	3.7009	0.7157	0.7867	1.3477
Indusion	0.8818	0.0573	0.0646	1.7353	86.4540	4.0657	0.7016	0.7503	0.5356
MF-HG	0.8246	0.0865	0.0973	1.9914	92.0446	4.3317	0.7058	0.7849	0.6943
SEGM	0.8369	0.0545	0.1148	2.6305	92.0395	4.3305	0.5761	0.6977	0.3670
Opt-Fus	0.8328	0.0850	0.0899	1.9961	84.5856	3.9799	0.6968	0.7972	2.2489

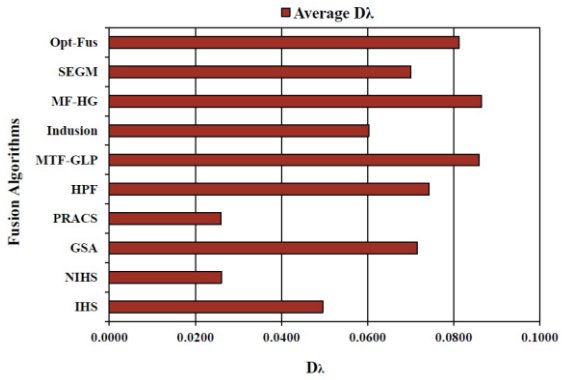

Fig. 4.Comparative measurement of average D_λ against all the image fusion algorithms.

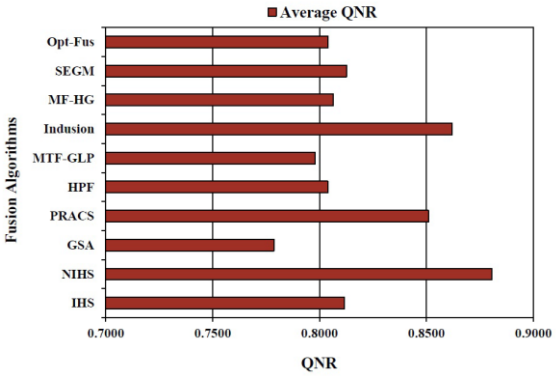

Fig. 6.Comparative measurement of average QNR against all the image fusion algorithms.

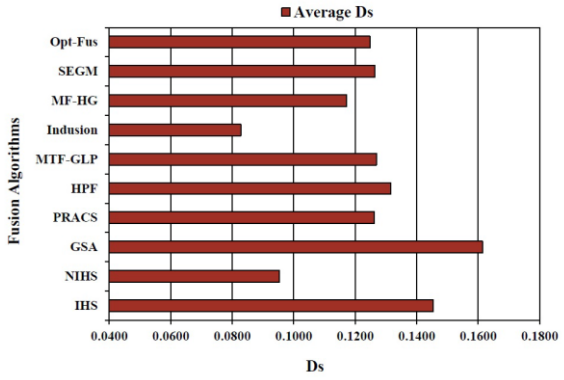

Fig. 5.Comparative measurement of average D_S against all the image fusion algorithms.

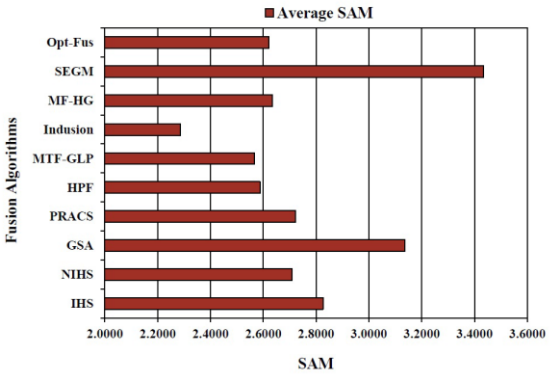

Fig. 7.Comparative measurement of average SAM against all the image fusion algorithms.

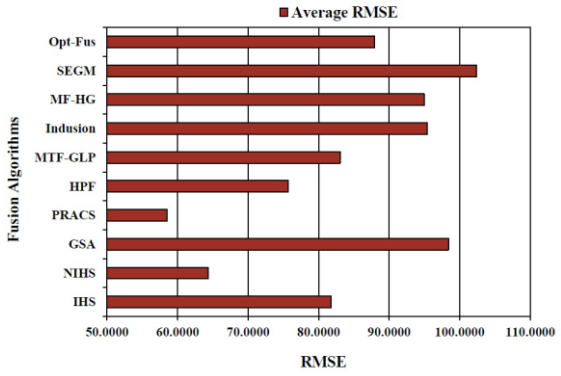

Fig. 8.Comparative measurement of average RMSE against all the image fusion algorithms.

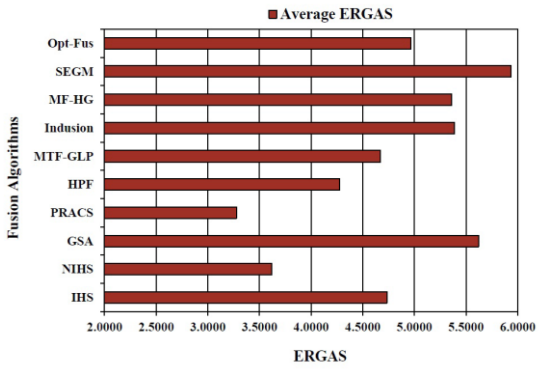

Fig. 9.Comparative measurement of average ERGAS against all the image fusion algorithms.

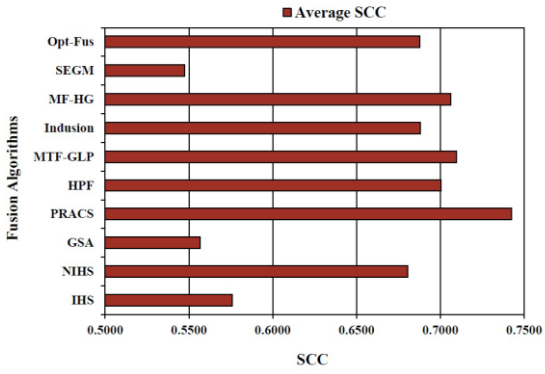

Fig. 10. Comparative measurement of average SCC against all the image fusion algorithms.

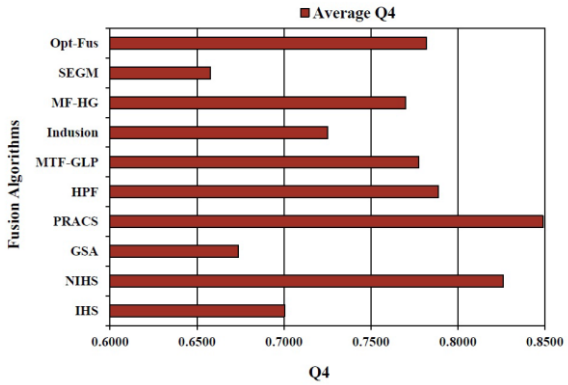

Fig. 11. Comparative measurement of average Q4 index against all the image fusion algorithms.

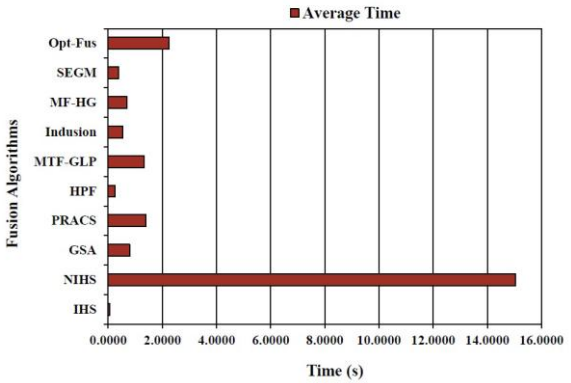

Fig. 12. Comparative measurement of average execution time against all the image fusion algorithms.

visual inspection of resultant images is necessary. It is observed that IHS results in spectral distortion in fused images. Comparatively, visualization of results look improved in the order HPF, MTF-GLP, MF-HG, SEGM, Opt-Fus, Indusion, GSA, PRACS. Despite of good values of objective metrics achieved by NIHS, it is observed with severe distortions and blur. Upon considering the overall spectral-spatial distortions along with clear distinction of objects, it is noted that visualization of Opt-Fus fused image is optimal among other resultant images.

V. CONCLUSION & FUTURE WORK

Use of optimization for producing efficient image fusion is attempted in this paper. This validation of the fusion algorithm now referred by 'Opt-Fus' is made possible while compared to nine other most recent image fusion algorithms from CS and MRA approaches. Two real datasets from WorldView-2 and WorldView-3 are utilized for this experimentation. To see the quantitative analysis along with visual inspection that helped in this wide comparison, following points are marked:

1) The performance of Opt-Fus algorithm is overall optimal among others. So, it is one of the application dependent alternatives for achieving image fusion.

2) The desired optimization of sensor relationship is computationally complex than other conventional algorithms. But, Opt-Fus is computationally very much economical than NIHS.

3) The increased availability of various optical imaging sensors those are characterized by different MTFs may challenge the universal acceptance of fusion algorithm.

4) The development of more adaptive algorithm that suits the most MTF values of source images will be a future work.

REFERENCES

1. X. Wang, S. Bai, Z. Li, R. Song, and J. Tao, "The PAN and MS image pansharpening algorithm based on adaptive neural network and sparse representation in the NSST domain," IEEE Access, vol. 7, pp. 2169–3536, 2019.
2. K. Zhang, M. Wang, S. Yang, and L. Jiao, "Convolution structure sparse coding for fusion of panchromatic and multispectral images," IEEE Trans. Geosci. Remote Sens., vol. 57, no. 02, pp. 1117–1130, Feb. 2019.
3. V. R. Pandit and R. J. Bhiwani, "Image fusion in remote sensing applications: A review," Int. J. Comput. Appl., vol. 120, no. 10, pp. 22–32, Jun. 2015.

4. G. Vivone et al., "A critical comparison among pansharpening algorithms," IEEE Trans. Geosci. Remote Sens., vol. 53, no. 5, pp. 2565–2586, May 2015.
5. C. Thomas, T. Ranchin, L. Wald, and J. Chanussot, "Synthesis of multispectral images to high spatial resolution: A critical review of fusion methods based on remote sensing physics," IEEE Trans. Geosci. Remote Sens., vol. 46, no. 5, pp. 1301–1312, May 2008.
6. V. R. Pandit and R. J. Bhiwani, "Component substitution based fusion of WorldView imagery," in Proc. IEEE The 10th Int. Conf. Comput., Commun. Netw. Technol. (ICCCNT), IIT, Kanpur, India, Jul. 2019.
7. V. R. Pandit and R. J. Bhiwani, "Fusion of QuickBird imagery using multi-resolution analysis based algorithms," in Proc. IEEE 4th Int. Conf. Commun. Electron. Syst. (ICCES), Coimbatore, India, Jul. 2019.
8. F. T. Mahmoudi, F. Samadzadegan, and P. Reinartz, "Object recognition based on the context aware decision-level fusion in multiviews imagery," IEEE J. Sel. Topics Appl. Earth Observ., vol. 8, no. 1, pp. 12–22, Jan. 2015.
9. B. Aiazzi et al., "Sensitivity of pansharpening methods to temporal and instrumental changes between multispectral and panchromatic data sets," IEEE Trans. Geosci. Remote Sens., vol. 55, no. 1, pp. 308–319, Jan. 2017.
10. I. R. Farah, W. Boulila, K. S. Ettabaˆa, B. Solaiman, and M. B. Ahmed, "Interpretation of multisensor remote sensing images: Multiapproach fusion of uncertain information," IEEE Trans. Geosci. Remote Sens., vol. 46, no. 12, pp. 4142–4152, Dec. 2008.
11. G. Vivone, P. Addesso, R. Restaino, M. D. Mura, and J. Chanussot, "Pansharpening based on deconvolution for multiband filter estimation," IEEE Trans. Geosci. Remote Sens., vol. 57, no. 1, pp. 540–553, Jan. 2019.
12. G. Vivone et al., "Pansharpening based on semiblind deconvolution," IEEE Trans. Geosci. Remote Sens., vol. 53, no. 4, pp. 1997–2010, Apr. 2015.
13. M. C. El-Mezouar, N. Taleb, K. Kpalma, and J. Ronsin, "An IHS based fusion for color distortion reduction and vegetation enhancement in IKONOS imagery," IEEE Trans. Geosci. Remote Sens., vol. 49, no. 5, pp. 5090–1602, May 2011.
14. M. Ghahremani and H. Ghassemian, "Nonlinear IHS: A promising method for pan-sharpening," IEEE Geosci. Remote Sens. Lett., vol. 13, no. 11, pp. 1606–1610, Nov. 2016.
15. B. Aiazzi, S. Baronti, and M. Selva, "Improving component substitution pansharpening through multivariate regression of MS+Pan data," IEEE Trans. Geosci. Remote Sens., vol. 45, no. 10, pp. 3230–3239, Oct. 2007.
16. R. Restaino, M. D. Mura, G. Vivone, and J. Chanussot, "Context adaptive pansharpening based on image segmentation," IEEE Trans. Geosci. Remote Sens., vol. 55, no. 2, pp. 753–766, Feb. 2017.
17. V. R. Pandit and R. J. Bhiwani, "Using image segmentation for fusion of multispectral to panchromatic imagery," in Proc. IEEE 5th Int. Conf. Image Inf. Process. (ICIIP), Waknaghat, India, Nov. 2019.
18. J. Pat S. Chavez, S. C. Sides, and J. A. Anderson, "Comparison of three different methods to merge multiresolution and multispectral data: Landsat TM and SPOT panchromatic," Photogramm. Eng. Remote Sens., vol. 57, no. 3, pp. 295–303, Mar. 1991.
19. B. Aiazzi, L. Alparone, S. Baronti, A. Garzelli, and M. Selva, "MTF tailored multiscale fusion of high-resolution MS and Pan imagery," Photogramm. Eng. Remote Sens., vol. 72, no. 5, pp. 591–596, May 2006.
20. J. Lee and C. Lee, "Fast and efficient panchromatic sharpening," IEEE Trans. Geosci. Remote Sens., vol. 48, no. 1, pp. 155–163, Jan. 2010.
21. B. Aiazzi, L. Alparone, S. Baronti, and A. Garzelli, "Context-driven fusion of high spatial and spectral resolution images based on oversampled multiresolution analysis," IEEE Trans. Geosci. Remote Sens., vol. 40, no. 10, pp. 2300–2312, Oct. 2002.
22. M. M. Khan, J. Chanussot, L. Condat, and A. Montanvert, "Indusion: Fusion of multispectral and panchromatic images using the induction scaling technique," IEEE Geosci. Remote Sens. Lett., vol. 5, no. 1, pp. 98–102, Jan. 2008.
23. R. Restaino, G. Vivone, M. D. Mura, and J. Chanussot, "Fusion of multispectral and panchromatic images based on morphological operators," IEEE Trans. Image Process., vol. 25, no. 6, pp. 2882–2895, Jun. 2016.
24. V. R. Pandit and R. J. Bhiwani, "Fusion of remote sensing imagery using morphological gradient," in Proc. IEEE 5th Int. Conf. Comput. Commun. Control Autom. (ICCUBEA), Pune, India, Sep. 2019.
25. (2016, May). [Online]. Available: https://www.digitalglobe.com/samples
26. (2019, Jul.). [Online]. Available: https://www.digitalglobe.com/samples
27. F. Palsson, J. R. Sveinsson, M. O. Ulfarsson, and J. A. Benediktsson, "Quantitative quality evaluation of pansharpened imagery: Consistency versus synthesis," IEEE Trans. Geosci. Remote Sens., vol. 54, no. 3, pp. 1247–1259, Mar. 2016.
28. S. Li and B. Yang, "A new pan-sharpening method using a compressed sensing technique," IEEE Trans. Geosci. Remote Sens., vol. 49, no. 2, pp. 738–746, Feb. 2011.
29. G. Vivone, R. Restaino, and J. Chanussot, "A bayesian procedure for full-resolution quality assessment of pansharpened products," IEEE Trans. Geosci. Remote Sens., vol. 56, no. 8, pp. 4820–4834, Aug. 2018.
30. L. He et al., "Pansharpening via detail injection based convolutional neural networks," IEEE J. Sel. Topics Appl. Earth Observ., vol. 12, no. 4, pp. 1188–1204, Apr. 2019.

AUTHORS PROFILE

Vaibhav R. Pandit received the Bachelor of Engineering (Electronics & Telecommunications) in 2009, Master of Engineering (Digital Electronics) in 2013 and is currently pursuing research in the domain of remote sensing image processing towards a Ph.D. degree from Sant Gadge Baba Amravati University, Maharashtra State, India. He is a student member of IEEE and its Geoscience and Remote Sensing Society, Associate Member of IEI, Associate Member of IETE and Life member of ISTE.

Dr. R. J. Bhiwani received the Bachelor of Engineering (Electronics Engineering) in 1988 from S.G.B. Amravati University, Master of Engineering (Instrumentation) in 1996 from B.A.M. University, Aurangabad and Ph.D. (Electronics & Telecommunication) in 2011 from S.R.T.M. University, Nanded located in Maharashtra State, India. He is currently working as Professor in the Department of Electronics and Telecommunication Engineering at Babasaheb Naik College of Engineering, Pusad, Maharashtra State, India. He has 30+ Years of wide experience in the engineering academics. He has authored several research papers published/presented at international and national levels. His research interests include Biomedical Engineering, Embedded System, Fuzzy Control, Image Processing, etc. He is a life member of professional bodies: ISTE, IE (I), IETE and ISOI.